Resonance Raman Spectroscopic Investigation of the Light-Harvesting Chromophore in *Escherichia coli* Photolyase and *Vibrio cholerae* Cryptochrome-1[†]

Olga Sokolova,[‡] Christine Cecala,[‡] Anand Gopal,[‡] Frank Cortazar,[§] Carla McDowell-Buchanan,[||] Aziz Sancar,[||] Yvonne M. Gindt,[§] and Johannes P. M. Schelvis*[,‡]

Department of Chemistry, New York University, New York, New York 10003, Department of Chemistry, Lafayette College, Easton, Pennsylvania 18042, and Department of Biochemistry and Biophysics, University of North Carolina School of Medicine, Chapel Hill, North Carolina 27599

Received November 17, 2006; Revised Manuscript Received January 25, 2007

ABSTRACT: Photolyases and cryptochromes are flavoproteins that belong to the class of blue-light photoreceptors. They usually bind two chromophores: flavin adenine dinucleotide (FAD), which forms the active site, and a light-harvesting pigment, which is a 5,10-methenyltetrahydrofolate polyglutamate (MTHF) in most cases. In *Escherichia coli* photolyase (EcPhr), the MTHF cofactor is present in substoichiometric amounts after purification, while in *Vibrio cholerae* cryptochrome-1 (VcCry1) the MTHF cofactor is bound more strongly and is present at stoichiometric levels after purification. In this paper, we have used resonance Raman spectroscopy to monitor the effect of loss of MTHF on the protein−FAD interactions in EcPhr and to probe the protein−MTHF interactions in both EcPhr and VcCry1. We find that removal of MTHF does not perturb protein−FAD interactions, suggesting that it may not affect the physicochemical properties of FAD in EcPhr. Our data demonstrate that the pteridine ring of MTHF in EcPhr has different interactions with the protein matrix than that of MTHF in VcCry1. Comparison to solution resonance Raman spectra of MTHF suggests that the carbonyl of its pteridine ring in EcPhr experiences stronger hydrogen bonding and a more polar environment than in VcCry1, but that hydrogen bonding to the pteridine ring amine hydrogens is stronger in VcCry-1. These differences in hydrogen bonding may account for the higher binding affinity of MTHF in VcCry1 compared to EcPhr.

Photolyases and cryptochromes are flavoproteins that belong to the family of blue-light photoreceptors (*1*−*3*). Photolyases use the energy of near-UV/blue-light photons to repair cyclobutane pyrimidine dimers (CPD[1]) and pyrimidine-(6-4)-pyrimidone photoproducts of DNA that are induced by UV light, and a specific photolyase exists for the repair of each of these photoproducts. In plants, cryptochromes use the same photons to regulate development and growth, while they are involved in entrainment of the circadian rhythm in animals. Despite a high degree of sequence and structural homology with CPD photolyase, no or marginal DNA repair activity has been reported for cryptochromes (*3*). However, a recent report shows that cryptochromes belonging to the cryptochrome-DASH (Cry-DASH) branch are actually photolyases with a high degree of specificity for CPD lesions in *single-stranded* DNA but contribute very little, if at all, to repair of genomic DNA (*4*). The Cry-DASH branch is composed of cryptochromes from bacterial, plant, and animal sources with higher sequence homology to *Drosophila* and human cryptochromes than bacterial photolyases and includes *Arabidopsis thaliana* cryptochrome-3 and *Synechocystis sp.* PCC6803 cryptochrome.

All photolyases and cryptochromes contain two noncovalently bound chromophores. One is always a flavin adenine dinucleotide (FAD), which is the catalytically active chromophore (*1*). The second chromophore functions as a light-harvesting pigment, which usually is 5,10-methenyltetrahydrofolate polyglutamate (MTHF), though some organisms synthesize and utilize 8-hydroxy-5-deazaflavin as the antenna pigment in these proteins (*1*).

In *Escherichia coli* photolyase (EcPhr)—a CPD photolyase—the light harvesting pigment is MTHF (*5*, *6*). The MTHF cofactor is partially lost during the isolation procedure and is present in substoichiometric amounts with respect to the FAD cofactor (*5*, *6*). MTHF and various of its derivatives can be used to reconstitute the enzyme (*6*−*8*). The MTHF cofactor can be removed from the enzyme completely by photodecomposition (*9*) or by reduction with sodium borohydride (*10*), while the E109A mutant of EcPhr does not

[†] This work was supported by New York University and NSF Grant MBC-0416511 (J.P.M.S.), NIH Grant GM31082 (A.S.), and the Lafayette College EXCEL Scholars Program (F.C.). Components of this work were conducted in a Shared Instrumentation Facility at NYU constructed with support from Research Facilities Improvement Grant No. C06 RR-16572 from the NCRR/NIH.

* To whom correspondence should be addressed: tel, (212) 998 3597; fax, (212) 260 7905; e-mail, hans.schelvis@nyu.edu.

[‡] New York University.

[§] Lafayette College.

[||] University of North Carolina School of Medicine.

[1] Abbreviations: CPD, cyclobutane pyrimidine dimer; AtCry3, *Arabidopsis thaliana* cryptochrome 3; DHB, 7,8-dihydrobiopterin; DHF, 7,8-dihydrofolate; EcPhr, *Escherichia coli* photolyase; FAD, flavin adenine dinucleotide; FADH•, neutral radical semiquinone of FAD; MTHF, 5,10-methenyltetrahydrofolate polyglutamate; $MTHF_{syn}$, 5,10-methenyltetrahydrofolic acid; RR, resonance Raman; VcCry1, *Vibrio cholerae* cryptochrome-1.

10.1021/bi602385j CCC: $37.00 © 2007 American Chemical Society
Published on Web 02/23/2007

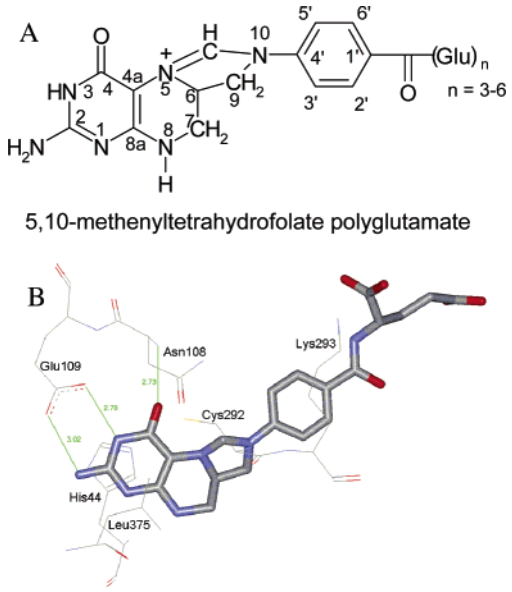

FIGURE 1: (A) Structure of 5,10-methenyltetrahydrofolate polyglutamate (MTHF) with atomic numbering. (B) Possible interactions between MTHF and amino acid residues in its binding pocket in EcPhr, PDB entry 1DNP (*17*).

bind the MTHF cofactor (*11*, *12*). During enzyme isolation and purification, the catalytic cofactor is oxidized to the neutral radical semiquinone FADH• (*13*, *14*), and further oxidation of the catalytic cofactor to FAD seemed to correlate to the extent of loss of MTHF (*15*), while photodecomposition studies also reported further oxidation of the FAD cofactor (*9*). MTHF is not required for DNA repair (*9*, *10*).

In recent resonance Raman studies on FADH• in EcPhr (*16*), we noticed an important difference between our data and those obtained for the MTHF-free E109A mutant (*11*). We proposed that removal of MTHF resulted in perturbation of FADH•−protein interactions, presumably hydrogen-bonding interactions, that could potentially result in facilitated oxidation of FADH•. MTHF is noncovalently bound to the protein mainly through hydrogen bonds with Glu109 and Asn108, while Cys292 may be involved in a charge interaction with the MTHF carbonyl, and Lys293 seems to form a salt bridge with the α-carboxylate of MTHF Glu-moiety (Figure 1) (*17*). In EcPhr, MTHF has three to six glutamates (*5*), which increase the binding affinity, presumably, by forming salt bridges with the protein (*18*). A recent site-directed mutagenesis study showed that mutation of these residues results in decreased binding of MTHF, but only the E109A mutation leads to complete loss of MTHF affinity (*12*). Since removal of the MTHF cofactor is a common practice for the study of electron-transfer processes in photolyase (e.g., refs *19*−*24*), it is important to know whether or not its removal affects the FAD binding pocket, its physicochemical properties, or both.

Vibrio cholerae cryptochrome 1 (VcCry1) is a member of the Cry-DASH branch and appears to have a high affinity for RNA (*25*). Recently, it has been discovered that the repair efficiency of CPD lesions in ssDNA and RNA by VcCry1 is very similar to that of the *V. cholerae* CPD photolyase (VcPhr) (*4*). However, the repair of CPD lesions in dsDNA by VcCry1 is only marginal compared to VcPhr and CPD photolyases in general, which repair CPD lesions in ssDNA and dsDNA with comparable efficiencies. Therefore, it has been proposed that VcCry1 and the other members of the Cry-DASH branch should be reclassified as ssDNA photolyases. VcCry1 binds both FAD and MTHF and is isolated with both molecules in near stoichiometric amounts, and FAD is present as a stable anionic hydroquinone ($FADH^-$) (*25*). This is in contrast with EcPhr, which is isolated with substoichiometric amounts of MTHF and with the FAD cofactor oxidized to its neutral radical semiquinone form (FADH•) (*6*). The strong binding of MTHF to VcCry1 makes it a good candidate for a comparative study with MTHF in EcPhr to shed more light onto the MTHF−protein interactions that determine the MTHF binding affinity.

In this work, we use resonance Raman (RR) spectroscopy to investigate the effect of MTHF removal and reconstitution on the neutral radical FAD (FADH•) of EcPhr. Although UV−vis spectroscopy has suggested that FAD_{ox} binds in a similar fashion to EcPhr in the absence of MTHF (*26*), RR spectroscopy is a much more sensitive probe of structural perturbations in biological molecules (*27*). Neither removal nor reconstitution of the enzyme with MTHF affects the vibrational spectrum of FADH•, and we conclude that the discrepancy between our previous results (*16*) and those of Murgida et al. (*11*) are not related to the MTHF stoichiometry and are probably due to perturbation of a hydrogen-bonding network that connects Glu109 to the N(3)-hydrogen of FADH•. We also noticed that the RR spectra of MTHF in water and in EcPhr are similar but show different H/D-exchange behavior. In contrast, the RR spectrum of MTHF in VcCry1 is more similar to that of MTHF in DMSO and has several Raman bands that show significant frequency shifts compared to EcPhr as well as different H/D-exchange behavior. These differences are discussed in light of the MTHF normal modes and differences in hydrogen bonding to and from MTHF in water, in EcPhr, and in VcCry1.

MATERIALS AND METHODS

Materials. DMSO-d_6 was purchased from Cambridge Isotope Laboratories. All other chemicals were purchased from Sigma-Aldrich and used without further purification.

Overexpression, Isolation, and Purification. The *E. coli* cells (strain pMS969) were grown and harvested, and the protein was isolated and purified as described previously (*14*, *16*). The overexpression, isolation, and purification of the maltose-binding protein (MBP)-fusion protein of *V. cholerae* cryptochrome-1 (VcCry1) have been described elsewhere (*25*). The purified enzyme was received in 50 mM Tris, pH 7.5, 100 mM NaCl, 1 mM EDTA, 5 mM DTT, and 50% glycerol and stored at −80 °C. For the RR experiments, glycerol was removed from the VcCry1 sample by using a desalting column.

Synthesis of 5,10-Methenyltetrahydrofolate ($MTHF_{syn}$). MTHF acid ($MTHF_{syn}$) was synthesized using the procedure of Rabinowitz (*28*). Ten milligrams of folinic acid was dissolved in 0.8 mL of 1 M β-mercaptoethanol, and the solution was titrated to pH 1.5 using 1 M HCl. The reaction mixture was covered and placed in the refrigerator at 4 °C for 24 h. The resulting yellow precipitate was filtered and then dissolved in 0.001 M HCl (pH 3). The amount of $MTHF_{syn}$ was determined from its absorption at $\lambda_{max} = 360$ nm ($\epsilon_{360} = 25\,100\ M^{-1}\ cm^{-1}$) (*28*). $MTHF_{syn}$ with its exchangeable hydrogens replaced with deuteriums, $MTHF_{syn}$-

(D), was prepared by performing the synthesis with D_2O as the solvent.

Removal of MTHF from E. coli Photolyase. MTHF was removed from EcPhr by using sodium borohydride (*10*). Briefly, 25 μL of 16 mM sodium borohydride in 50 mM sodium borate at pH 9.5 was added to 500 μL of EcPhr (200 μM) in 50 mM HEPES, 0.4 M K_2SO_4 at pH 7.4 and left to react for 30 min on ice. The removal of MTHF was monitored by the disappearance of its absorption band at 380 nm.

Reconstitution of DNA Photolyase with MTHF$_{syn}$. EcPhr was reconstituted with a stoichiometric amount of MTHF by incubation of purified enzyme with 2- to 4-fold excess $MTHF_{syn}$ (in 0.001 M HCl) in 50 mM potassium phosphate, pH 7.4, and 4.8 mM DTT overnight at 4 °C. After incubation, the reconstituted samples were centrifuged at 4 °C using a Centricon YM-30 centifugal filter (Millipore) to remove the excess $MTHF_{syn}$. Alternatively, the purified enzyme was titrated with 10 μM aliquots of $MTHF_{syn}$ (in 0.001 M HCl) in 50 mM potassium phosphate, pH 7.4. After addition of each aliquot, the sample was left covered on ice for 20 min. The fully reconstituted enzyme was centrifuged at 4 °C using a Centricon YM-30 centifugal filter (Millipore) to remove the excess $MTHF_{syn}$. In each case, progress of reconstitution was monitored by UV−vis spectroscopy. Both methods gave the same result.

Electronic Absorption and Resonance Raman Spectroscopy. Electronic absorption spectra were recorded at room temperature with a Lambda P40 UV−vis spectrophotometer (Perkin-Elmer). The RR spectra were obtained with the home-built instrument described elsewhere (*16*). The samples were excited with 350.7, 530.9, or 568.2 nm light from a Kr^+-laser (I-302, Coherent) with 10 mW laser power at the sample. Laser plasma lines were removed with a fused-silica Pellin-Broca prism (Lambda Research Optics, Inc.) or with 3 nm band-pass filters (Omega Optical). The Rayleigh scattered light was suppressed by using appropriate holographic notch filters (Kaiser Optical). The samples (200 μL) were placed in a Raman spinning cell and cooled to 6 ± 2 °C during the experiments by a flow of cold N_2 gas to avoid laser heating of the samples. After 30 min of laser excitation, EcPhr and VcCry1 showed negligible signs of degradation as judged from absorption and RR spectra taken before and after the experiments. Excitation of EcPhr at 350.7 nm did result in rapid photodegradation of the MTHF cofactor (*7*, *9*, *19*) and concomitant oxidation of the FAD cofactor within 10 min of laser irradiation as judged from the appearance of the 1576 cm^{-1} Raman band of oxidized flavin (*29*). Therefore, EcPhr samples were replaced after 5 min of laser exposure at 350.7 nm before the appearance of the 1576 cm^{-1} band. The RR spectra were corrected for a sloping, luminescent background by subtracting a polynomial function, and toluene was used to calibrate the spectra. The slit width of the instrument was 3 cm^{-1}, and Raman frequencies were determined with a reproducibility of better than 1 cm^{-1}.

FT-IR Spectroscopy. FT-IR spectra of $MTHF_{syn}$ and $MTHF_{syn}$(D) in KBr pellets were obtained with an Avatar 360 FT-IR spectrometer (Thermo Electron Corporation) and a resolution of 4 cm^{-1}.

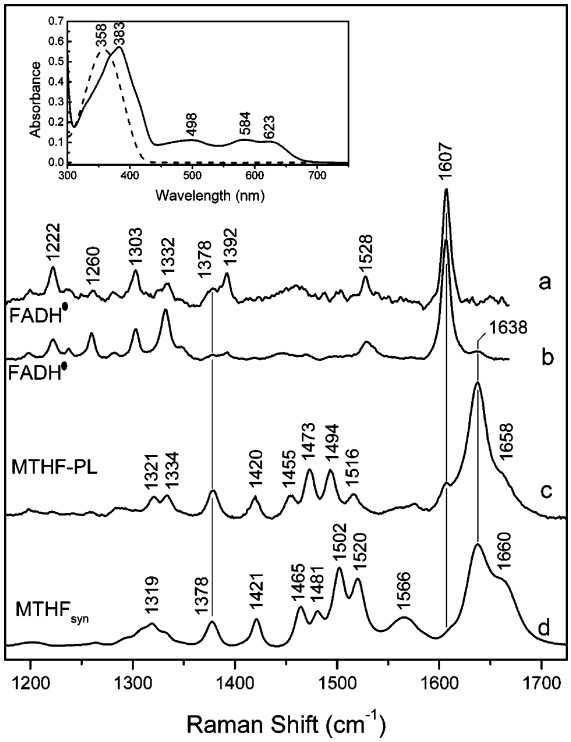

FIGURE 2: Resonance Raman spectra of FADH• (a, b) and MTHF (c) in EcPhr and of $MTHF_{syn}$ (d) that were obtained with 568.2 nm (a), 530.9 nm (b), and 350.7 nm (c, d) excitation. The enzyme was in 50 mM HEPES, 0.4 M K_2SO_4 at pH 7.4 at a concentration of 200 μM (a, b) and of 100 μM (c), and $MTHF_{syn}$ was in H_2O with 0.001 M HCl at pH 3. The laser power was 10 mW with a 30 min accumulation time, while spectrum c is the average of several 5 min accumulations of different samples. Inset: Absorption spectra of EcPhr (solid line) and of $MTHF_{syn}$ in 0.001 M HCl (dashed line).

RESULTS

Identification of MTHF and FADH• Raman Bands in E. coli Photolyase. We used selective excitation to identify the Raman bands that are associated with the MTHF cofactor. The inset in Figure 2 shows the absorption spectrum of EcPhr. The broad absorption band at 383 nm is largely due to the MTHF cofactor with minor contributions from FADH•, and the absorption above 450 nm is entirely due to FADH• (*13*, *14*). Figure 2 shows the RR spectra of EcPhr with selective excitation of FADH• at 530.9 and 568.2 nm and of MTHF at 350.7 nm. The spectrum of FADH• in EcPhr has been described in detail elsewhere and is characterized by an intense band at 1607 cm^{-1}, and a relatively weak one at 1638 cm^{-1} (*16*). When MTHF is directly excited at 350.7 nm, the RR spectrum is completely different from the FADH• spectrum; the 1638 cm^{-1} band becomes dominant, while the characteristic 1607 cm^{-1} peak of FADH• is barely visible. Other intense bands occur at 1516, 1494, 1473, 1455, 1420, and 1378 cm^{-1}, and a shoulder is observed at 1658 cm^{-1}. The absorption spectrum of synthesized MTHF ($MTHF_{syn}$) in H_2O (pH 3) is shown in the inset of Figure 2 (dashed line) and is blue-shifted by 25 nm with respect to MTHF in EcPhr. In this paper, $MTHF_{syn}$ in H_2O or D_2O refers to H_2O or D_2O with 0.001 M HCl at pH 3. The RR spectrum of $MTHF_{syn}$ in H_2O excited at 350.7 nm is very similar to that of MTHF in EcPhr with bands at 1638, 1520, 1502, 1481, 1465, 1421, and 1378 cm^{-1}, while the shoulder at 1660 cm^{-1} is more distinct, and a broad feature is observed at 1566 cm^{-1}. The similarities between these spectra of

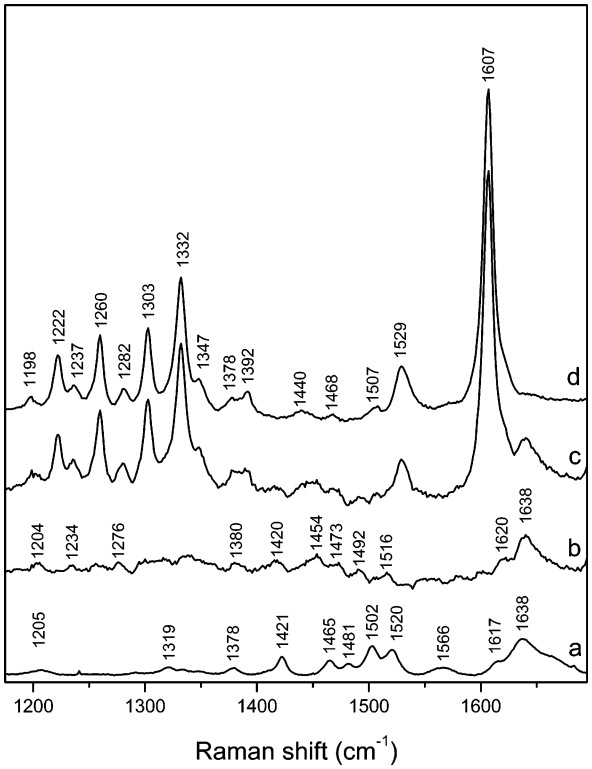

FIGURE 3: Raman spectrum of $MTHF_{syn}$ in water with 0.001 M HCl (a) and of MTHF in dithionite reduced EcPhr (b), and resonance Raman spectrum of EcPhr (c). (d) The resonance Raman spectrum of pure FADH• in EcPhr obtained after subtraction of spectrum b ($FADH^-$ and MTHF) from spectrum c (FADH• and MTHF) after normalization of the spectra on the 1638 cm^{-1} band. All spectra were obtained with 530.9 nm excitation and 10 mW laser power. The EcPhr concentration was 400 μM (b) and 200 μM (c) in 20 mM phosphate buffer, pH 7.0, and 0.4 M K_2SO_4.

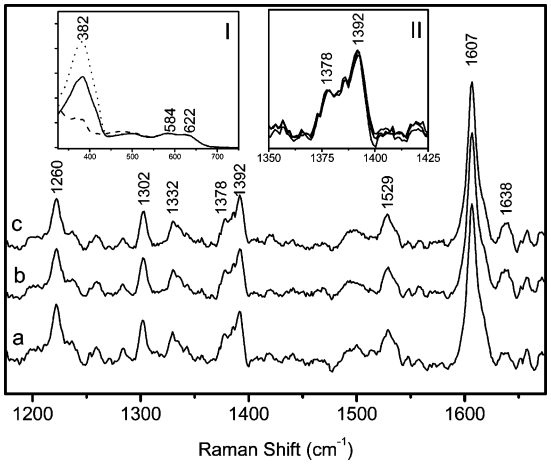

FIGURE 4: Resonance Raman spectra of EcPhr (200 μM) in 50 mM HEPES, 0.4 M K_2SO_4 at pH 7.4 after removal of MTHF (a), as isolated (b), and after reconstitution with $MTHF_{syn}$ (c) that were obtained with 568.2 nm excitation and 10 mW laser power. The spectra were normalized on the intensity of the 1607 cm^{-1} vibration. Inset I: Absorption spectra of EcPhr after removal of MTHF (dashed line), as isolated (solid line), and after reconstitution with $MTHF_{syn}$ (dotted line). Inset II: Enlargement of the 1350−1425 cm^{-1} region of the overlaid resonance Raman spectra of EcPhr shown in Figure 4.

MTHF in EcPhr and $MTHF_{syn}$ in H_2O confirm our assignment of spectrum 2c to that of the MTHF cofactor in EcPhr.

To identify the contributions of MTHF to the RR spectrum FADH• in EcPhr, we obtained the Raman spectrum of $MTHF_{syn}$ in H_2O and of EcPhr in 0.4 M K_2SO_4 and 20 mM phosphate at pH 7 with 530.9 nm excitation. Phosphate buffer was used to avoid buffer contributions to the spectrum above 1100 cm^{-1}. In Figure 3, we show the Raman spectrum of $MTHF_{syn}$ in H_2O (pH 3) obtained with 530.9 nm excitation (trace a), which is similar to the spectrum obtained with 350.7 nm excitation (Figure 2d). The Raman spectrum of MTHF in EcPhr with 530.9 nm excitation was collected through reduction of FADH• to $FADH^-$ by addition of a small excess of dithionite with the sample under a nitrogen atmosphere. Since Raman scattering of reduced flavins is very weak (*30*), we expect to observe only the MTHF Raman spectrum. Although the spectrum is very weak (trace b), the Raman bands occur at the same frequencies as with 350.7 nm excitation (Figure 2c), but with slightly different relative intensities. The difference spectrum (trace d) that is obtained after subtraction of the MTHF Raman spectrum (trace b) from the RR spectrum of FADH• in EcPhr (trace c) upon normalization with the 1638 cm^{-1} band reveals FADH• Raman bands at 1507, 1468, and 1440 cm^{-1} that are otherwise obscured by MTHF and buffer contributions (*16*). The difference spectrum has a better signal-to-noise because systematic noise in both spectra (traces b and c) due to the etaloning effect of the detector is canceled by the subtraction. Three new Raman bands were recently reported for FADH• in *A. thaliana* (6-4)-photolyase in D_2O buffer at 1536, 1508, and 1456 cm^{-1}, and it was proposed that they coincidently overlaid into one band at 1522 cm^{-1} in H_2O buffer (*31*). However, the equivalent 1529 cm^{-1} band of FADH• in EcPhr is not sensitive to H/D-exchange (*16*). We propose that the 1507 cm^{-1}, and 1468 or 1440 cm^{-1} bands in EcPhr in H_2O buffer are the ordinary counterparts of the 1508 and 1456 cm^{-1} bands of FADH• in *A. thaliana* (6-4)-photolyase in D_2O buffer. After correction for MTHF contributions, the 1378 cm^{-1} band is still present and clearly arises from FADH• and not from MTHF as we originally proposed (*16*). The RR spectrum of FADH• in *A. thaliana* (6-4)-photolyase, which lacked MTHF, has a 1398 cm^{-1} band with a shoulder at 1391 cm^{-1} and a weak band at 1374 cm^{-1} (*31, 32*). However, it is not clear whether any of these bands correspond to the 1378 cm^{-1} band of FADH• in EcPhr.

Removal of MTHF from E. coli Photolyase and Its Reconstitution with $MTHF_{syn}$. To determine whether the presence of MTHF has any effect on FADH• in EcPhr, we prepared MTHF-free EcPhr, and we reconstituted purified EcPhr with $MTHF_{syn}$ to obtain a 1:1 stoichiometry of FAD and MTHF. Inset I in Figure 4 shows the absorption spectra of EcPhr as isolated (solid line), with MTHF removed (dashed line), and reconstituted with $MTHF_{syn}$ (dotted line). We estimate that our purified EcPhr has an FADH•:MTHF stoichiometry of 1.0:0.69 (0.69 ± 0.01) by using an extinction coefficient of 25 900 M^{-1} cm^{-1} for MTHF and of 6000 M^{-1} cm^{-1} for FADH• at 380 nm and of 4800 M^{-1} cm^{-1} for FADH• at 580 nm (*6, 7*). The FADH•:MTHF stoichiometry in the reconstituted sample is 1.0:1.14 (1.14 ± 0.15). Figure 4 shows the RR spectra of purified EcPhr, MTHF-free EcPhr, and purified EcPhr reconstituted with $MTHF_{syn}$. These spectra are obtained with 568.2 nm excitation, which significantly enhances the 1378 cm^{-1} band and allows for direct comparison to the RR spectrum of the MTHF-free E109A mutant of EcPhr which lacks the 1378 cm^{-1} band (*11*). The noise in the spectra is again due to the

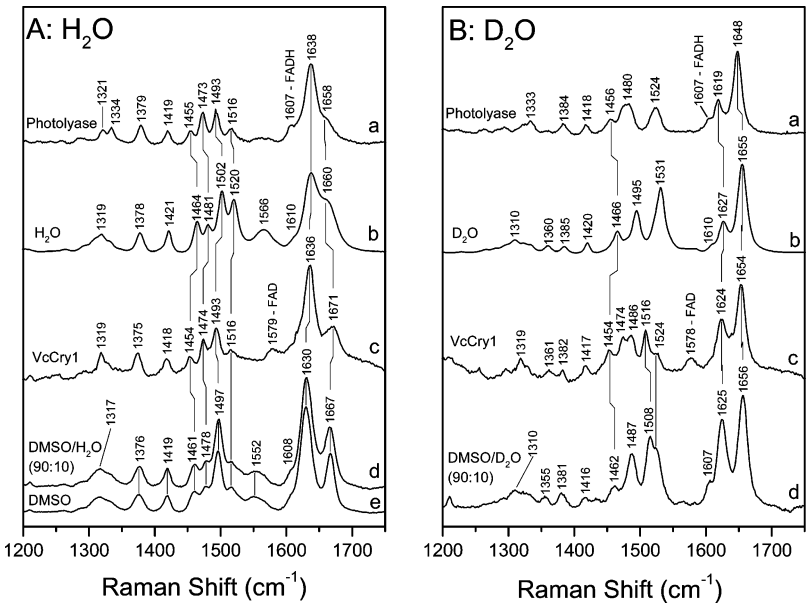

FIGURE 5: (A) Resonance Raman spectra of MTHF in EcPhr (100 μM) in 50 mM HEPES, pH 7.4, and 0.4 M K_2SO_4 (a), $MTHF_{syn}$ in H_2O (0.001 M HCl) (b), MTHF in VcCry1 (100 μM) in 50 mM Tris, pH 7.5, 100 mM NaCl, 1 mM EDTA (c), and 5 mM DTT, and $MTHF_{syn}$ in DMSO:H_2O (90:10 v/v) (d) and in DMSO (e). (B) MTHF in EcPhr in D_2O buffer (a), $MTHF_{syn}$ in D_2O (b), MTHF in VcCry1 in D_2O buffer (c), and $MTHF_{syn}$ in DMSO:D_2O (90:10 v/v) (d). Excitation was at 350.7 nm with 10 mW laser power.

etaloning effect of the CCD detector. All three spectra are basically identical except for the weak MTHF band at 1638 cm^{-1}, and the enlarged spectral region (inset II) shows clearly that the 1378 cm^{-1} band is insensitive to the stoichiometry of the MTHF cofactor in EcPhr. Excitation at 530.9 nm gave similar results, but the intensity of the 1378 cm^{-1} band is much weaker at this excitation wavelength (data not shown). Therefore, we conclude that the 1378 cm^{-1} band is solely due to FADH• without any significant contribution of MTHF. Although the RR spectrum of FADH• is very sensitive to substrate binding (*16*, *32*), it is not affected at all by the presence or absence of MTHF, which indicates that removal of MTHF perturbs neither the FADH• binding pocket nor, most likely, the physicochemical properties of FADH•.

Resonance Raman Spectroscopy of MTHF in Different Environments. The spectra in Figure 2 show that some of the Raman frequencies of MTHF in EcPhr and of $MTHF_{syn}$ in H_2O are quite different. This is most likely due to differences in hydrogen-bonding interactions and in polarity of the MTHF environment. For further exploration, we obtained the RR spectra of MTHF in EcPhr and in *V. cholerae* cryptochrome-1 (VcCry1) in H_2O and D_2O buffer. VcCry1 is of interest because it tightly binds MTHF and is isolated with stoichiometric amounts of MTHF bound in contrast with EcPhr (*25*). For comparison, we also obtained spectra of $MTHF_{syn}$ in H_2O and D_2O, and in DMSO, and in DMSO/H_2O or DMSO/D_2O (90:10 v/v). DMSO ($\epsilon_r = 48$) is less polar than water ($\epsilon_r = 78.5$) and only acts as a weak hydrogen-bond acceptor; it cannot function as a hydrogen-bond donor. A comparative study in H_2O and DMSO was successfully performed to gain further insight into hydrogen bonding between riboflavin and water and to identify the carbonyl stretching vibration of 7,8-dihydrofolate and 7,8-dihydrobiopterin (*33*−*35*), which are structurally related to MTHF.

Figure 5A shows the RR spectra of MTHF in EcPhr, in H_2O, in VcCry1, in DMSO/H_2O (90:10 v/v), and in DMSO. The spectra are relatively similar with two main spectral regions from 1600 to 1750 cm^{-1} and from 1350 to 1550 cm^{-1}. The most significant differences occur in the former region, where MTHF in EcPhr and $MTHF_{syn}$ in H_2O have the most intense band at 1638 cm^{-1} with a shoulder at 1658 and 1660 cm^{-1}, respectively. MTHF in VcCry1 and $MTHF_{syn}$ in DMSO have the most intense band at 1636 and 1630 cm^{-1}, respectively, with a distinct separate band at 1671 and 1667 cm^{-1}, respectively. In the 1350−1550 cm^{-1} region, MTHF in EcPhr and VcCry1 has very similar Raman frequencies, which are generally lower than those of $MTHF_{syn}$ in DMSO and in H_2O. However, the 1379 cm^{-1} band in EcPhr occurs at 1378 cm^{-1} in H_2O, and at 1375 and 1376 cm^{-1} in VcCry1 and DMSO, respectively. The Raman frequencies are listed in Table 1 for comparison. The 1607 cm^{-1} band in EcPhr is due to FADH• (*16*), and the 1579 cm^{-1} band in VcCry1 is due to a small amount of oxidized FAD (*25*, *29*). The RR spectra of $MTHF_{syn}$ in DMSO and in DMSO/H_2O (90:10 v/v) are identical, indicating that doping DMSO with H_2O or D_2O (90:10 v/v) does not noticeably change the solvent properties of DMSO, though we cannot rule out that DMSO contains a trace amount of water.

The four exchangeable hydrogens of the MTHF pteridine ring (Figure 1) give rise to complex changes in the MTHF spectra in D_2O solutions, and the differences between MTHF in EcPhr and in VcCry1 are significant (Figure 5B). The bands at 1654 and 1624 cm^{-1} in VcCry1 are similar to those of $MTHF_{syn}$ in D_2O and DMSO/D_2O (90:10 v/v) but occur at a 5−6 cm^{-1} lower frequency in EcPhr. Between 1460 and 1530 cm^{-1}, *four* distinct bands are observed in VcCry1, which seem to melt together into *two* broader bands in EcPhr. In the same region, $MTHF_{syn}$ in DMSO/D_2O (90:10 v/v) and in D_2O has *three* and *two* distinct bands, respectively. Although the Raman bands of MTHF in EcPhr in the 1600−1750 cm^{-1} region are different from the other samples, its spectrum between 1350 and 1550 cm^{-1} is similar to that of $MTHF_{syn}$ in D_2O. The spectrum of MTHF in VcCry1 in D_2O

Table 1: Raman Frequencies (cm^{-1}) of MTHF in *E. coli* Photolyase (EcPhr), in *V. cholerae* Cryptochrome-1 (VcCry1), in Water (0.001 M HCl), and in DMSO-d_6 Obtained by Resonance Raman Spectroscopy and of MTHF in KBr Pellet from FT-IR Experiments

EcPhr	VcCry1	H_2O	DMSO	FT-IR	tentative assignment[a]
				1727	νCO (Glu)
1658	1671	1660	1667	1663	νC=O, νC=N$^+$, δNH$_{(2)}$
1638	1636	1638	1630	1640[b]	νC=N$^+$, νC=O, δNH$_{(2)}$
		1610	1608		ν_{8a}, benzoyl
1607[a]					FADH•
				1602	ν_{8b}, benzoyl
	1579[b]				FAD$_{ox}$
		1566	1552	1560	na[c]
1516	1516	1520	1516	1545/1506[b]	na
1493	1493	1502	1497	1493	na
1473	1474	1481	1478	1475	na
1455	1454	1464	1461	1453	na
1419	1418	1421	1419	1412[b]	na
1379	1375	1378	1376	1374	na
1334	1327	1330	1331		na
1321	1319	1319	1317	1316	na

[a] Assignment as discussed in the text, only proposed dominant contributor to mode is indicated. [b] These FT-IR vibrations do not necessarily correspond to the Raman vibrations in the same row. [c] No assignment attempted.

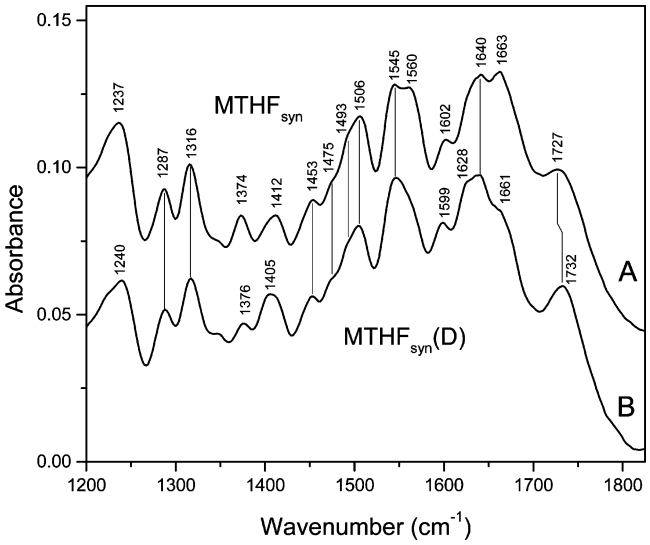

FIGURE 6: FT-IR spectra of solid $MTHF_{syn}$ (A) and $MTHF_{syn}$ with its exchangeable hydrogens substituted with deuteriums, $MTHF_{syn}$-(D) (B), in KBr pellet.

buffer has more in common with that of $MTHF_{syn}$ in DMSO/D_2O (90:10 v/v).

Overall, the Raman spectrum of MTHF in EcPhr behaves more similarly to that of $MTHF_{syn}$ in H_2O, while that of MTHF in VcCry1 corresponds better to that of $MTHF_{syn}$ in DMSO. We believe that this observation reflects differences in polarity of the MTHF binding pocket and in hydrogen-bonding environment and strength of MTHF in EcPhr and VcCry1. Another important observation is that MTHF in EcPhr undergoes photodecomposition with 350.7 nm excitation concomitant with oxidation of FADH• to FAD, while for VcCry1 neither photodecomposition of MTHF nor oxidation of $FADH^-$ was observed.

Figure 6 shows the FT-IR spectra of $MTHF_{syn}$ and of $MTHF_{syn}$ with its exchangeable hydrogens replaced with deuteriums ($MTHF_{syn}$(D)). Unlike the RR spectra that show mainly the Raman-active bands of the pteridine/imidazolinium moiety of MTHF, the FT-IR spectra show all IR-active bands of MTHF. New, IR-active bands are observed in the 1200−1350 cm^{-1} and 1500−1600 cm^{-1} regions and at 1727 cm^{-1}. The latter band is isotope sensitive and is most likely due to a CO stretching vibration. The broad band between 1600 and 1700 cm^{-1} shows a little isotope sensitivity; a band at 1663 cm^{-1} loses intensity, while one at 1628 cm^{-1} gains intensity in $MTHF_{syn}$(D).

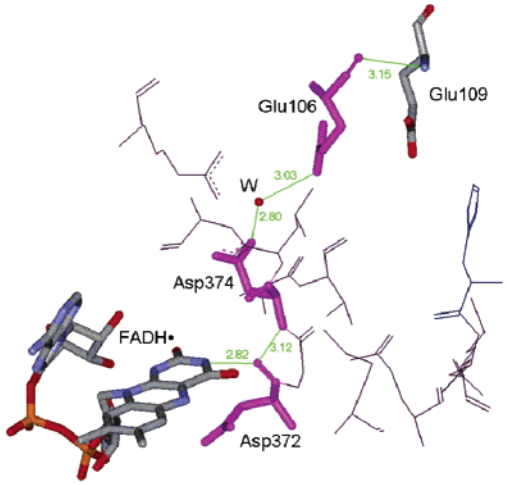

FIGURE 7: Proposed hydrogen-bonding network (green lines) that connects Glu109 and the N(3)H of FADH• in EcPhr. The residues in the network are in magenta, and PDB entry 1DNP was used to construct the figure (*17*). W = water. The hydrogen bond (3.2 Å) between the amide hydrogen of Asp374 and the C4 carbonyl of FADH• has been omitted for clarity.

DISCUSSION

Effect of MTHF on the Protein Environment of FAD in E. coli Photolyase. In a previous study, we observed a Raman band at 1378 cm^{-1} that was absent in the MTHF-free E109A mutant of EcPhr and that could be a potential marker band for the perturbation of FADH•−protein interactions (*11*, *16*). In this work, we have demonstrated that the 1378 cm^{-1} band is not due to MTHF but originates from FADH• in EcPhr. Neither removal of MTHF from nor $MTHF_{syn}$-reconstitution of isolated EcPhr affects the 1378 cm^{-1} band in particular and the RR spectrum of FADH• in general. Therefore, we conclude that MTHF removal does neither perturb FADH•−protein interactions nor, most likely, the physicochemical properties of the FAD cofactor, in agreement with previous UV−vis spectroscopic and activity studies of flavin- and pterin-reconstituted EcPhr (*7*, *26*). Our findings do not support our hypothesis that MTHF may have a structural role to protect FADH• against air-oxidation to FAD (*16*).

An alternative explanation for the absence of the 1378 cm^{-1} band in the MTHF-free E109A-mutant of EcPhr may be that the E109A substitution results in minor perturbation of the protein conformation, including the FAD binding pocket and protein−FADH• interactions. Glu109 is the most important residue for binding of MTHF (*12*). Its carboxylate group accepts two hydrogen bonds from MTHF and is about 13 Å away from the C4 carbonyl of FADH• (*18*). Figure 7 shows a possible hydrogen-bonding network between Glu109 and FADH• that starts with a hydrogen bond between the Glu109 amide hydrogen and the Glu106 backbone carbonyl. A water molecule forms a hydrogen-bond bridge between the Glu106 and Asp 374 carboxylate groups. The amide

hydrogen of Asp374 forms hydrogen bonds with the C4 carbonyl of FADH• and with the backbone carbonyl of Asp372, which forms a hydrogen bond with the N3 hydrogen of FADH•. Therefore, it is possible that substitution of Glu109 with alanine triggers a small change in this hydrogen-bonding network, which perturbs the hydrogen-bonding interactions between Asp372 and Asp374 and FADH•. Since Asp372 interacts with the FADH• N3 hydrogen and the 1378 cm^{-1} vibration is sensitive to H/D exchange (*16*), disruption of this interaction is more likely to affect the 1378 cm^{-1} band in the E109A mutant. Although our data show that removal of MTHF alone does not affect the FADH•−protein interactions, we cannot rule out that the lack of MTHF enhances the allosteric effect of the E109A substitution.

MTHF Environment in E. coli Photolyase and in VcCry1. To interpret the RR spectra of MTHF in terms of its interactions with the protein, it is important to understand its vibrational normal modes, but normal mode assignments are not yet available for MTHF. Significant work has been done on 7,8-dihydrobiopterin (DHB) and 7,8-dihydrofolate (DHF) by Callender and co-workers (*34*−*36*). Although these molecules do not have the unique imidazolinium ring of MTHF, the assignment of their pteridine ring modes will facilitate the interpretation of the MTHF Raman spectra. Furthermore, DHB and DHF exhibit a similar binding motif in proteins as MTHF in EcPhr, i.e., the N2−C2−N3 part of the pteridine ring forms hydrogen bonds with either a glutamate or an aspartate residue (*35*, *37*, *38*).

The MTHF Raman spectrum is characterized by a broad band between 1600 and 1750 cm^{-1} and a region from 1350 to 1530 cm^{-1} that includes six well-resolved bands. We will focus on the broad band which has likely contributions from νC═O, νC═N^+, δNH, and the NH_2 scissor (δNH_2) vibrations and will be sensitive to hydrogen bonding. In this spectral region, we assign the 1727 cm^{-1} band in the FT-IR spectrum to νCO of the glutamate group (*39*), because the amide I vibration of folate molecules and the νC═O of a pteridine or pyrimidine are expected below 1700 cm^{-1} (*34*, *35*, *40*, *41*).

We assign the shoulder at 1660 cm^{-1} of $MTHF_{syn}$ in H_2O to νC═O of the pteridine ring because of its shift to 1667 cm^{-1} in DMSO, which is analogous to the behavior of νC═O of DHB in these solvents (*35*). Subsequently, we assign the 1671 cm^{-1} band and the 1658 cm^{-1} shoulder of MTHF in VcCry1 and in EcPhr, respectively, to νC═O. It has a lower frequency than νC═O in guanosine (*41*), and its Raman intensity is significant. Therefore, we propose some coupling of νC═O with νC═N^+. Since this band is sensitive to H/D-exchange, we expect that δNH and δNH_2 vibrations also contribute to this normal mode. In D_2O, νC═O shifts to 1627 cm^{-1}, which is supported by the FT-IR data of $MTHF_{syn}$(D) that show the disappearance of the 1663 cm^{-1} band and the appearance of a shoulder at 1628 cm^{-1}, which is very similar to the behavior of νC═O of DHB in D_2O (*35*).

On the basis of the following observations, we attribute the intense MTHF Raman band at 1638 cm^{-1} to νC═N^+ with contributions from δ(NH), δNH_2, and νC═O. In ethidium, νC═N^+ is coupled to δNH_2 and occurs around 1626 and 1629 cm^{-1} in H_2O and D_2O, respectively (*42*, *43*), and at 1683 cm^{-1} in $[(CH_3)_2N{=}CH_2]^+$, shifting to 1648 cm^{-1} upon deuteration of the methylene group (*44*). Therefore, the uncoupled νC═N^+ vibration falls between 1629 and 1648 cm^{-1}, and coupling of νC═N^+ with δ(NH) and/or δNH_2 may change its frequency in MTHF. The contribution of δNH and δNH_2 to the 1638 cm^{-1} band is supported by its significant shift to 1655 cm^{-1} in D_2O. Furthermore, the 1638 cm^{-1} band of MTHF shifts to 1630 cm^{-1} in DMSO. This behavior is very similar to the νC5═N mode of DHB (*33*), which is coupled to νC═O and δNH (*35*). The positive charge of the iminium is probably delocalized over the N5═C−N atoms of the imidazolinium ring of MTHF (*12*, *45*), which may lower the intensity of this vibration in the FT-IR spectrum and be responsible for the lower frequency of νC═N^+ in MTHF compared to νC═N of DHF and DHB in solution and bound to protein (*34*−*36*) by reducing the C═N^+ bond order, though coupling of different vibrations with νC═N^+ cannot be ruled out.

The weak 1608 cm^{-1} Raman band of $MTHF_{syn}$ in H_2O does not shift in D_2O, while the 1602 cm^{-1} IR-band shifts to 1599 cm^{-1} for $MTHF_{syn}$(D). Therefore, we assign the 1608 and 1602 cm^{-1} bands to the ν_{8a} and ν_{8b} modes, respectively, of the benzoyl ring following the assignment for similar molecules with a *p*-amino-benzoyl-L-glutamate moiety (*40*, *46*). Although δNH_2 has been reported between 1680 and 1700 cm^{-1} for guanine and guanosine (*41*, *47*) and shifts down by more than 400 cm^{-1} for δND_2 (*41*, *48*), we do not observe this vibration for MTHF. This is probably due to its coupling to νC═N^+ and νC═O as described above, while IR-bands from the *p*-amino-benzoyl-L-glutamate moiety, e.g., the amide I mode, may obscure δNH_2 in the 1600−1700 cm^{-1} region of the FT-IR spectrum.

Preliminary density functional theory calculations with the B3LYP functional and 6-31G(d,p) basis set on truncated MTHF with H at the 1′ position suggest that the normal modes with the five highest frequencies are νC═O with δ(N3H) contribution, two modes each with contributions from δNH_2, νC═N^+, and δN3H, and two modes located on the benzoyl ring (O. Sokolova and J. P. M. Schelvis, unpublished results). After H/D-exchange, only four normal modes are predicted by the calculations—νC═O, νC═N^+, and the two benzoyl modes—and δN3D and δND_2 are completely uncoupled from νC═O and νC═N^+. These preliminary calculations support our assignment of the MTHF vibrations in the 1600 to 1750 cm^{-1} region, except for coupling between νC═O and νC═N^+. However, hydrogen bonding to the carbonyl oxygen presumably lowers the νC═O frequency to allow for coupling with νC═N^+. Additional experiments on isotopically labeled MTHF and more sophisticated *ab initio* calculations to account for hydrogen bonding will be necessary to establish a better picture of the MTHF normal modes.

We will now use the MTHF normal mode assignments and the recently resolved crystal structure of *A. thaliana* cryptochrome-3 (AtCry3) to analyze the differences in MTHF−protein interactions in EcPhr and VcCry1 (*49*). AtCry3 is a single-stranded DNA-specific photolyase of the Cry-DASH branch, and sequence alignment suggests that AtCry3 is a good model for MTHF binding in VcCry1 (*4*, *49*, *50*). In AtCry3, 13 residues interact with MTHF, five of which interact through formation of eight hydrogen bonds (*49*). In contrast, only six residues interact with MTHF in EcPhr, four of which participate in six hydrogen bonds (*17*,

49). First, the frequency of the band with predominant νC═O character is similar in EcPhr and in H_2O, while it occurs at higher frequencies in DMSO and VcCry1. This suggests that the pteridine carbonyl of MTHF experiences a less polar environment and/or weaker hydrogen bond in VcCry1 than in EcPhr. In AtCry3, Glu149 (Asp110 in VcCry1) donates one 2.9 Å hydrogen bond to the pteridine carbonyl of MTHF, while Asn108 forms two hydrogen bonds (2.7 and 3.0 Å) to this carbonyl in EcPhr (*17*, *49*). Furthermore, the proximity of the Glu149 carboxylate provides a more negatively charged environment for the pteridine carbonyl in AtCry3. The differences in hydrogen-bonding and polar environment of the pteridine carbonyl between AtCry3 and EcPhr are in perfect agreement with the observed behavior and our interpretation of νC═O in VcCry1 and EcPhr. Second, the proposed νC═O and νC═N^+ occur around 1625 and 1655 cm^{-1}, respectively, for MTHF in D_2O and in VcCry1 in D_2O buffer, and at least at 5 cm^{-1} lower frequencies in EcPhr in D_2O buffer. By assuming that δND and δND_2 are effectively uncoupled from νC═O and νC═N^+ in D_2O, we can estimate that the effect of coupling of δNH and δNH_2 on νC═N^+ is similar in all three cases, -17 to -20 cm^{-1}. However, the coupling effect on νC═O is different at $+33$, $+41$, and $+46$ cm^{-1} for H_2O, EcPhr, and VcCry1, respectively. Since hydrogen bonding raises the frequency of δNH_2 and of vibrations coupled to δNH (*33*, *51*, *52*), hydrogen bonding to NH and NH_2 of MTHF seems stronger in VcCry1 than in EcPhr and H_2O. In AtCry3, Glu150, Tyr423, and Glu417 (Glu111, Tyr371, and Glu365 in VcCry1) participate in six hydrogen bonds with the pteridine ring, while only Glu109 participates in two hydrogen bonds with the MTHF pteridine ring in EcPhr (*17*, *49*). In EcPhr, there are no equivalents for the total of three hydrogen bonds between N1 and Tyr423 and N8-H and Glu417 in AtCry3. This is in excellent agreement with our predictions of more and/or stronger hydrogen bonding to MTHF in VcCry1 compared to EcPhr.

In summary, we propose that hydrogen bonding to the C4 carbonyl of MTHF is weaker and to N3H, N8H, and NH_2 of MTHF is stronger in VcCry1 than in EcPhr, resulting in a higher affinity of MTHF for VcCry1. The X-ray crystal structure of AtCry3 supports our analysis, especially, because its hydrogen-bonding residues are conserved in VcCry1. The differences in hydrogen bonding between MTHF in VcCry1 and EcPhr may also explain the lack of photodecomposition of MTHF in VcCry1 by modifying the MTHF reduction potential.

CONCLUSION

We have shown that the removal of the MTHF cofactor from EcPhr does not result in perturbation of the FAD binding pocket, and we propose that it does not affect the physicochemical properties of the FAD cofactor. We hypothesize that the E109A mutation, which results in loss of MTHF affinity of EcPhr, causes small changes in a hydrogen-bonding network between Glu109 and the FAD cofactor that are observed as small differences in the RR spectra of FADH• in EcPhr and its E109A mutant.

We have recorded RR spectra of the MTHF cofactor and have proposed normal mode assignments for the 1600−1750 cm^{-1} region, which is sensitive to hydrogen-bonding interactions. This part of the spectrum of MTHF in VcCry1 is different from that in EcPhr, and comparison to $MTHF_{syn}$ in H_2O and in DMSO suggests that its pteridine carbonyl experiences a less polar environment and has a weaker hydrogen bond, if any, with the protein matrix in VcCry1 than in EcPhr. On the other hand, hydrogen bonding to the amine hydrogens of MTHF seems stronger in VcCry1 than in EcPhr. These differences in hydrogen bonding may be responsible for the tighter binding of MTHF in VcCry1 than in EcPhr. Our analysis is supported by the MTHF hydrogen-bonding environment in AtCry3 and indicates that MTHF most likely experiences a very similar protein environment in VcCry1.

ACKNOWLEDGMENT

We thank Prof. Johann Deisenhofer for making his paper available to us prior to its publication.

REFERENCES

1. Sancar, A. (2003) Structure and function of DNA photolyase and cryptochrome blue-light photoreceptors, *Chem. Rev. 103*, 2203−37.
2. Cashmore, A. R., Jarillo, J. A., Wu. Y. J., and Liu, D. (1999) Cryptochromes: blue light receptors for plants and animals, *Science 284*, 760−5.
3. Partch, C. L., and Sancar, A. (2005) Photochemistry and photobiology of cryptochrome blue-light photopigments: the search for a photocycle, *Photochem. Photobiol. 81*, 1291−1304.
4. Selby, C. P., and Sancar, A. (2006) A cryptochrome/photolyase class of enzymes with single-stranded DNA-specific photolyase activity, *Proc. Natl. Acad. Sci. U.S.A. 103*, 17696−700.
5. Johnson, J. L., Hamm-Alvarez, S., Payne, G., Sancar, G. B., Rajagopalan, K. V., and Sancar, A. (1988) Identification of the second chromophore of Escherichia coli and yeast DNA photolyase as 5,10-methenyltetrahydrofolate, *Proc. Natl. Acad. Sci. U.S.A. 85*, 2046−50.
6. Wang, B., and Jorns, M. S. (1989) Reconstitution of Escherichia coli DNA photolyase with various folate derivatives, *Biochemistry 28*, 1148−52.
7. Jorns, M. S., Wang, B., Jordan, S. P., and Chanderkar, L. P. (1990) Chromophore function and interaction in Escherichia coli DNA photolyase: reconstitution of the apoenzyme with pterin and/or flavin derivatives, *Biochemistry 29*, 552−61.
8. Lipman, R. S. A., and Jorns, M. S. (1996) An unnatural folate stereoisomer is catalytically competent in DNA photolyase, *Biochemistry 35*, 7968−73.
9. Heelis, P. F., Payne, G., and Sancar, A. (1987) Photochemical properties of Escherichia coli DNA photolyase: selective photodecomposition of the second chromophore, *Biochemistry 26*, 4634−40.
10. Jorns, M. S., Wang, B., and Jordan, S. P. (1987) DNA repair catalyzed by Escherichia coli DNA photolyase containing only reduced flavin: elimination of the enzyme's second chromophore by reduction with sodium borohydride, *Biochemistry 26*, 6810−6.
11. Murgida, D. H., Schleicher, E., Bacher, A., Richter, G., and Hildebrandt, P. (2001) Resonance Raman spectroscopic study of the neutral flavin radical complex of DNA photolyase from Escherichia coli, *J. Raman Spectrosc. 32*, 551−6.
12. Henry, A. A., Jimenez, R., Hanway, D., and Romesberg, F. E. (2004) Preliminary characterization of light harvesting in E. coli DNA photolyase, *ChemBioChem 5*, 1088−94.
13. Jorns, M. S., Sancar, G. B., and Sancar, A. (1984) Identification of a neutral flavin radical and characterization of a second chromophore in Escherichia coli DNA photolyase, *Biochemistry 23*, 2673−9.
14. Gindt, Y. M., Vollenbroek, E., Westphal, K., Sackett, H., Sancar, A., and Babcock, G. T. (1999) Origin of the transient electron paramagnetic resonance signals in DNA photolyase, *Biochemistry 38*, 3857−66.
15. Jorns, M. S., Baldwin, E. T., Sancar, G. B., and Sancar, A. (1987) Action mechanism of Escherichia coli DNA photolyase, *J. Biol. Chem. 262*, 486−91.

16. Schelvis, J. P. M., Ramsey, M., Sokolova, O., Tavares, C., Cecala, C., Connell, K., Wagner, S., and Gindt, Y. M. (2003) Resonance Raman and UV-Vis spectroscopic characterization of the complex of photolyase with UV-damaged DNA, *J. Phys. Chem. B 107*, 12352−62.
17. Park, H.-W., Kim, S.-T., Sancar, A., and Deisenhofer, J. (1995) Crystal structure of DNA photolyase from Escherichia coli, *Science 268*, 1866−72.
18. Hamm-Alvarez, S., Sancar, A., and Rajagopalan, K. V. (1990) The folate cofactor of Escherichia coli DNA photolyase acts catalytically, *J. Biol. Chem. 265*, 18656−62.
19. Li, Y. F., Heelis, P. F., and Sancar, A. (1991) Active site of DNA photolyase: tryptophan-306 is the intrinsic hydrogen atom donor essential for flavin radical photoreduction and DNA repair in vitro, *Biochemistry 30*, 6322−29.
20. Okamura, T., Sancar, A., Heelis, P. F., Begley, T. P., Hirata, Y., and Mataga, N. (1991) Picosecond laser photolysis studies on the photorepair of pyrimidine dimers by DNA photolyase. 1. Laser photolysis of photolyase-2-deoxyuridine dinucleotide photodimer complex, *J. Am. Chem. Soc. 113*, 3143−5.
21. Kim, S. T., Heelis, P. F., Okamura, T., Hirata, Y., Mataga, N., and Sancar, A. (1991) Determination of rates and yields of interchromophore (folate → flavin) energy transfer and intermolecular (flavin → DNA) electron transfer in Escherichia coli DNA photolyase by time-resolved fluorescence and absorption spectroscopy, *Biochemistry 30*, 11262−70.
22. Aubert, C., Vos, M. H., Mathis, P., Eker, A. P. M., and Brettel, K. (2000) Intraprotein radical transfer during photoactivation of DNA photolyase, *Nature 405*, 586−90.
23. MacFarlane, A. W., IV, and Stanley, R. J. (2003) *Cis-syn* thymidine dimer repair by DNA photolyase in real time, *Biochemistry 42*, 8558−68.
24. Kao, Y.-T., Saxena, C., Wang, L., Sancar, A., and Zhong, D. (2005) Direct observation of thymine dimer repair in DNA by photolyase, *Proc. Natl. Acad. Sci. U.S.A. 102*, 16128−32.
25. Worthington, E. N., Kavakli, I. H., Berrocal-Tito, G., Bondo, B. E., and Sancar, A. (2003) Purification and characterization of three members of the photolyase/cryptochrome family blue-light photoreceptors from Vibrio cholerae, *J. Biol. Chem. 278*, 39143−54.
26. Payne, G., Wills, M., Walsh, C., and Sancar, A. (1990) Reconstitution of Escherichia coli photolyase with flavins and flavin analogues, *Biochemistry 29*, 5706−11.
27. Spiro, T. G., Ed., (1988) Biological Applications of Raman Spectroscopy, John Wiley & Sons, New York.
28. Rabinowitz, J. C. (1963) Preparation and properties of 5,10-methenyltetrahydrofolic acid and 10-formyltetrahydrofolate, *Methods Enzymol. 6*, 814−5.
29. Bowman, W. D., and Spiro, T. G. (1981) Normal mode analysis of lumiflavin and interpretation of resonance Raman spectra of flavoproteins, *Biochemistry 20*, 3313−8.
30. Zheng, Y., Carey, P. R., and Palfey, B. A. (2004) Raman spectrum of fully reduced flavin, *J. Raman Spectrosc. 35*, 521−4.
31. Li, J., Uchida, T., Ohta, T., Todo, T., and Kitagawa, T. (2006) Characteristic structure and environment in FAD cofactor of (6-4) photolyase along function revealed by resonance Raman spectroscopy, *J. Phys. Chem. B 110*, 16724−32.
32. Li, J., Uchida, T., Todo, T., and Kitagawa, T. (2006) Similarities and differences between cyclobutane pyrimidine dimer photolyase and (6-4) photolyase as revealed by resonance Raman spectroscopy. Electron transfer from the FAD cofactor to ultraviolet-damaged DNA, *J. Biol. Chem. 281*, 25551−9.
33. Schmidt, J., Coudron, P., Thompson, A. W., Watters, K. L., and McFarland, J. T. (1983) Hydrogen bonding between flavin and protein: a resonance Raman study, *Biochemistry 22*, 76−84.
34. Deng, H., Callender, R., and Howell, E. (2001) Vibrational structure of dihydrofolate bound to R67 dihydrofolate reductase, *J. Biol. Chem. 276*, 48956−60.
35. Deng, H., Callender, R., and Dale, G. E. (2000) A vibrational structure of 7,8-dihydrobiopterin bound to dihydroneopterin aldolase, *J. Biol. Chem. 275*, 30139−43.
36. Deng, H., and Callender, R. (1998) Structure of dihydrofolate when bound to dihydrofolate reductase, *J. Am. Chem. Soc. 120*, 7730−7.
37. Bystroff, C., Oatley, S. J., and Kraut, J. (1990) Crystal structure of Escherichia coli dihydrofolate reductase: the $NADP^+$ holoenzyme and the folate · $NADP^+$ ternary complex. Substrate binding and a model for the transition state, *Biochemistry 29*, 3263−77.
38. Hennig, M., D'Arcy, A., Hampele, I. C., Page, M. G. P., Oefner, C., and Dale, G. E. (1998) Crystal structure and reaction mechanism of 7,8-dihydroneopterin aldolase from Staphylococcus aureus, *Nat. Struct. Biol. 5*, 357−62.
39. Tsuboi, M. (1962) Infrared dichroism and molecular conformation of α-form poly-γ-benzyl-L-glutamate, *J. Polym. Sci. 59*, 139−53.
40. Austin, J. C., Fitzhugh, A., Villafranca, J. E., and Spiro, T. G. (1995) Stereoelectronic activation of methylenetetrahydrofolate by thymidylate synthase: resonance Raman spectroscopic evidence, *Biochemistry 34*, 7678−85.
41. Toyama, A., Hanada, N., Ono, J., Yoshimitsu, E., and Takeuchi, H. (1999) Assignment of guanosine UV resonance Raman bands on the basis of ^{13}C, ^{15}N and ^{18}O substitution effects, *J. Raman Spectrosc. 30*, 623−30.
42. Benevides, J. M., and Thomas, Jr., G. J. (2005) Local conformational changes induced in B-DNA by ethidium intercalation, *Biochemistry 44*, 2993−9.
43. Luedtke, N. W., Liu, Q., and Tor, Y. (2005) On the electronic structure of ethidium, *Chem. Eur. J. 11*, 495−508.
44. Clark, G. R., Shaw, G. L., Surman, P. W. J., Taylor, M. J., and Steele, D. (1994) Preparation, structure and vibrational spectrum of the dimethylmethyleniminium ion, including the role of cationic polymers in its formation, *J. Chem. Soc., Faraday Trans. 90*, 3139−44.
45. Khalifa, E., Bieri, J. H., and Viscontini, M. (1979) Konformationsanalyse von 5,10-methenyl-(6*RS*)-5,6,7,8-tetrahydro-L-folsäure, *Helv. Chim. Acta 62*, 1340−4.
46. Ozaki, Y., King, R. W., and Carey, P. R. (1981) Methotrexate and folate binding to dihydrofolate reductase. Separate characterization of the pteridine and p-aminobenzoyl binding sites by resonance Raman spectroscopy, *Biochemistry 20*, 3219−25.
47. Mathlouthi, M., Seuvre, A. M., and Koenig, J. L. (1986) F.T.-I.R. and laser-Raman spectra of guanine and guanosine, *Carbohydr. Res. 146*, 15−27.
48. Miura, T., and Thomas, Jr., G. J. (1995) Structure and dynamics of interstrand guanine association in quadruplex telomeric DNA, *Biochemistry 34*, 9645−54.
49. Huang, Y., Baxter, R., Smith, B. S., Partch, C. L., Colbert, C. L., and Deisenhofer, J. (2006) Crystal structure of cryptochrome 3 from Arabidopsis thaliana and its implications for photolyase activity, *Proc. Natl. Acad. Sci. U.S.A. 103*, 17701−6.
50. Kleine, T., Lockhart, P., and Batschauer, A. (2003) An Arabidopsis protein closely related to Synechocystis cryptochrome is targeted to organelles, *Plant J. 35*, 93−103.
51. Borisenko, V. E., Krekov, S. A., Guzemin, A. G., and Koll, A. (2003) The influence of hetero-substitution in the aromatic ring of amino pyrimidine on amino group characteristics in free and H-bonded molecules, *J. Mol. Struct. 646*, 125−40.
52. Lively, C. R., and McFarland, J. T. (1990) Assignment and the effect of hydrogen bonding on the vibrational normal modes of flavins and flavoproteins, *J. Phys. Chem. 94*, 3980−94.

BI602385J